Flavor Singlet Contribution to the Structure Function g_1 at Small-x

J. Bartels[1]

II. Institut für Theoretische Physik, Universität Hamburg

B.I.Ermolaev[2]

A.F.Ioffe Physical-Technical Institute, St.Petersburg, 194021, Russia

M. G. Ryskin[3]

Petersburg Nuclear Physics Institute, Gatchina, St.Petersburg, 188350, Russia

Abstract: The singlet contribution to the $g_1(x, Q^2)$ structure function is calculated in the double-logarithmic approximation of perturbative QCD in the region $x \ll 1$. Double logarithmic contributions of the type $(\alpha_s \ln^2(1/x))^k$ which are not included in the GLAP evolution equations are shown to give a power-like rise at small-x which is much stronger than the extrapolation of the GLAP expressions. The dominant contribution is due to the gluons which, in contrast to the unpolarized case, mix with the fermions also in the region $x \ll 1$. The two main reasons why the small-x behavior of the double logarithmic approximation is so much stronger than the usual GLAP evolution are: the larger kinematical region of integration (in particular, no ordering in transverse momentum) and the contributions from non-ladder diagrams.

1 Introduction

The investigation of the structure functions g_1 and g_2 provides the basis for the theoretical description of polarization effects in deep inelastic lepton nucleon scattering. Particular interest has been given to the behavior of g_1 at small x: experimental data [1] on both g_1^P and g_1^N are limited to $x > 10^{-2}$, and numerical values of the moments $\Gamma^{P,N} = \int_0^1 dx g_1^{P,N}$ therefore depend upon the extrapolation in the region $x < 10^{-2}$.

In QCD the Q^2 evolution at not too small x of g_1 is, like in the unpolarized case, described by the GLAP-evolution equations [2, 3]. The prediction for the small-x behavior is that both the quark and the gluon polarized structure functions go as

$$\Delta q(x, Q^2), \Delta g(x, Q^2) \sim \exp \sqrt{const \cdot \alpha_s \ln(Q^2/\mu^2) \ln(1/x)}. \tag{1.1}$$

In particular, in the flavor singlet part the gluons and the quarks mix. In a recent paper [4] it has been shown, for the flavor nonsinglet contribution to g_1, that this simple double log extrapolation (1) of the GLAP evolution equations, in fact, strongly underestimates the rise at small x. The reason is that, at $x \ll 1$, new double logarithmic contributions appear which are beyond the control of the standard evolution framework. To be more precise, in the region of not too small x where the standard analysis applies the leading behavior in the n-th order of α_s is of the type

$$(\alpha_s \ln(Q^2/\mu^2))^n [a_n(\ln(1/x))^n + a_{n-1}(\ln(1/x)^{n-1} + ...] \tag{1.2}$$

(where μ denotes the renormalization scale, and for simplicity we restrict ourselves to a fixed α_s), whereas at very small x the dominant contributions are of the form:

$$(\alpha_s \ln(1/x) \ln(1/x))^n. \tag{1.3}$$

These double logarithmic contributions are not included in the standard evolution scheme [3]. In [4] the sum of the double logarithms

$$(\alpha_s)^n [b_n(\ln(1/x))^{2n} + b_{n-1}(\ln(1/x))^{2n-1} \ln(Q^2/\mu^2) + ... + b_0(\ln(1/x))^n(\ln(Q^2/\mu^2))^n \tag{1.4}$$

has been shown to give rise to a power-like increase of the flavor nonsinglet structure function at small-x which is stronger than the GLAP predicition (1).

In this paper we continue our investigation of the small-x behavior of g_1 in the double logarithmic approximation, by calculating the flavour singlet contribution. Like in the flavor nonsinglet case, we derive and solve evolution equations which describe the dependence upon the infrared cutoff of the transverse momentum integrations. Our main results is the power-like growth of g_1 at small-x (eqs.(4.21) - (4.23)). A discussion of the phenomenological implications of our result will be presented in a forthcoming paper.

2 Singlet contribution to g_1 in lowest orders α_s

Let us consider the scattering process where the off-shell photon with momentum q $(-q^2 = Q^2 > 0)$ strikes the polarized quark with momentum p. We assume that the total energy is much greater than the mass of the quark, m.

$$s = 2pq >> m^2. \tag{2.1}$$

We follow the notation of [4, 5] and introduce the scattering amplitudes T_i in the following way:

$$
\begin{aligned}
T_{\mu\nu} &= \imath \int d^4x e^{\imath qx} < N|T\left(J_\mu(x)J_\nu(0)\right)|N> \\
&= (-g_{\mu\nu} + \frac{q_\mu q_\nu}{q^2})T_1 + (p_\mu - q_\mu\frac{pq}{q^2})(p_\nu - q_\nu\frac{pq}{q^2})T_2 \\
&\quad + \imath\epsilon_{\mu\nu\alpha\beta}q^\alpha s^\beta\frac{m}{pq}T_3 + \imath\epsilon_{\mu\nu\alpha\beta}q^\alpha(s^\beta(pq) - p^\beta(sq))\frac{m}{pq}T_4.
\end{aligned}
\tag{2.2}
$$

The structure function g_1 is defined as

$$g_1 = -\frac{1}{2\pi}ImT_3. \tag{2.3}$$

In the Born approximation the matrix element for this process is given by the Feynman graphs in Fig 1. Let us denote by $M_L(M_R)$ the matrix element for the case when the initial quark has left (the right) helicity. Then we obtain

$$T_3^{Born} = \frac{M_L^{Born} - M_R^{Born}}{2} = e_q^2(\frac{s}{s - Q^2 + \imath\epsilon} - \frac{-s}{-s - Q^2 + \imath\epsilon}) \tag{2.4}$$

so that

$$g_1^{Born} = -\frac{1}{2\pi}ImM^{Born}. \tag{2.5}$$

e_q here stands for the electric charge of the initial quark. Expession (2.4) shows that T_3^{Born} is antisymmetrical with respect to replacing s by $-s$, i.e. in terms of the Regge theory T_3^{Born} has negative/odd signature. QCD radiative corrections turn T_3^{Born} into T_3. As usual, it consists of the flavor nonsinglet part T_3^{NS} and the flavour singlet part T_3^S. The small-x behavior of the nonsinglet contribution has been discussed in [4], and in this paper we shall consider the singlet part. All Feynman graphs contributing to the double-logarithmic approximation (DLA) of the nonsinglet part T_3^{NS} can be obtained from the graphs in Fig.1 by adding the gluon lines (further rungs and nonladder bremsstrahlungs gluons). An example is shown in Fig.2. In the present case of the flavor singlet we will have to include more general contributions, in particular gluon ladders. An example is shown in Fig.3. As a result, we first have to consider the four different types of kernels: ΔP_{qq}, ΔP_{qg}, ΔP_{gq}, and ΔP_{gg}. They will be derived in the remainder of this section and agree with the limit $x \to 0$

of the leading order splitting functions of [3]. In addition to these expressions for the kernels, we find the region of integration which gives the double logarithmic contributions. Next we will have to consider the bremsstrahlungs gluons. As the result of this section, we obtain all the ingreduents for the infrared evolution equations that will be discussed in the following section. Throughout this paper we will use the Feynman gauge and the Sudakov representation for the quark and gluon momenta:

$$k_1 = \alpha_i q' + \beta_i p + k_{Ti}, \tag{2.6}$$

$$q' = q + xp, \tag{2.7}$$

and

$$dk_i = \frac{s}{4} d\alpha_i d\beta_i dk_{Ti}^2 d\varphi_i. \tag{2.8}$$

For the beginning let us briefly review [4] the structure of the double log contribution in the non-singlet case. The imaginary part of the amplitude T_3 comes from the s-channel graph Fig.1, and the spin structure of (M_L-M_R), corresponding to the quark line has the form

$$tr\left[\gamma_5\hat{p}\gamma_\mu(\hat{q}+\hat{p})\gamma_\nu\right] = -4i\varepsilon_{\mu\nu\alpha\beta}q^\alpha p^\beta, \quad \left(\gamma_5 = -i\varepsilon_{\alpha\beta\gamma\delta}\gamma^\alpha\gamma^\beta\gamma^\gamma\gamma^\delta\right). \tag{2.9}$$

which coincides with the tensor $i\varepsilon_{\mu\nu\alpha\beta}q^\alpha s^\beta \cdot m$ in eq.(2.2) for the longitudinal spin vector $s^\beta = p^\beta/m$ of the initial quark. To obtain the leading logarithm in the first loop Fig.2a, one has to cancel one of the two transverse momenta factors k_t^2 from the t-channel quark propagators. In the trace

$$tr\left[\gamma_5\hat{p}\gamma_{\alpha'}\hat{k}\gamma_\mu(\hat{q}+\hat{k})\gamma_\nu\hat{k}\gamma_{\alpha'}\right] \simeq 2tr\left[\gamma_5\hat{p}\hat{k}\gamma_\mu\hat{q}'\gamma_\nu\hat{k}\right] \tag{2.10}$$

we have to keep the largest momentum q' in the s-channel quark propagator $(\hat{q}+\hat{k})$, and retain only the transverse components of the photon polarization vectors (μ and ν) (see eq. (2.9)). Therefore one can omit the $\alpha q'_\mu$ component of k_μ

$$tr\left[\ldots\alpha\hat{q}'\hat{q}'\ldots\right] = \alpha q'^2 tr\left[\ldots\right] = 0 \quad as \quad q'^2 = 0 \tag{2.11}$$

and write

$$2tr\left[\gamma_5\hat{p}\hat{k}\gamma_\mu\hat{q}'\gamma_\nu\hat{k}\right] = 2k_t^2 tr\left[\gamma_5\hat{p}\gamma_\mu\hat{q}\gamma_\nu\right]. \tag{2.12}$$

Together with the quark propagators $(1/k_t^2)^2$ and the colour factor $C_F = (N_c^2 - 1)/2N_c$ it gives the logarithmic loop integral:

$$\frac{2C_F}{4\pi}\alpha_s\frac{dk_t^2}{k^4} \cdot k_t^2 \tag{2.13}$$

4

The same reasoning is valid for the second loop fig.2b [6]. As a result, we obtain for the gluon rung inside the fermion ladder ΔP_{qq}:

$$\Delta P_{qq} = C_F. \tag{2.14}$$

This result is also valid for the flavor singlet.

Turning now to the singlet case, in the second loop approximation a new type of diagrams appears, contributions with t-cannel gluons. The first diagram of this type, Fig.3, contains two fermion traces. The lower one, originating from the initial quark spinors, has the form eq.(2.9) with the gluon momentum $(-k^\alpha)$ instead of q^α. It is antisymmetric in the polarizations of the two gluons with momentum k_1. Thus we cannnot assign the same (longitudinal) polarizations to both gluons: otherwise we would have $M_R = M_L$ and $T_3 = \frac{1}{2}(M_L - M_R) = 0$. The best one can do in order to retain the largest power of $1/x$ (in the small x region) is to assign the longitudinal polarization $e_\mu \propto q'_{\mu'}$ to one of the two gluon and the transverse polarization $(e'_\nu = e_{\nu't})$ to the other gluon. In the proton (quark) rest frame with $k_{1t} = k_x$ this means that $e_{\mu'} = e_z$, $e_{\nu'} = e_y$, and the lower trace

$$tr_l = -tr\left(\gamma_5 \hat{p} \hat{e}_{\mu'} \hat{k}_1 \hat{e}_{\nu'}\right) = 4i\varepsilon_{\mu'\nu'\alpha\beta}k_{1t}^\alpha p^\beta = -4ie_{z\mu'}|p \parallel k_{1t}|e_{y\nu'}. \tag{2.15}$$

To obtain the logarithmic integration over k_1 we have to find another factor k_{1t} from the upper trace, i.e. to take the component $\hat{k}_{1t}$ in the quark propagator $(\hat{k}_2 - \hat{k}_1)$ — the only one, which contains the momentum k_{1t}. The product of three γ-matrices $\hat{e}_{\mu'}$, $\hat{k}_{1t}\hat{e}_{\nu'}$, in the upper trace may be written as

$$\hat{e}_{\mu'z}\hat{k}_{1tx}\hat{e}_{\nu'y} = -i\gamma_5\gamma_0|k_{1t}| \quad . \tag{2.16}$$

Therefore the trace corresponding to the fermion loop in Fig.3 takes the same form (2.10) as for the Fig.2b

$$\sim tr\left[\gamma_5 \hat{p} \hat{k}_2 \gamma_\mu \hat{q} \gamma_\nu \hat{k}_2\right], \tag{2.17}$$

and in this way the polarization of the target quark is transfered to the fermion loop. So the upper quark loop can be calculated in analogy with the one-loop graph in Fig.2a. As usual, the DL-contribution comes from the kinematical region of

$$1 \gg \beta_1 \gg \beta_2 \gg \ldots \tag{2.18}$$

and

$$\ldots \ll \alpha_1 \ll \alpha_2 \ll 1. \tag{2.19}$$

where all the s-channel (horizontal lines) particles are on mass shell.[4] In this case $\alpha_i\beta_i s \ll k_{it}^2$, so $k_i^2 \approx k_{it}^2$.

---

[4]The ordering $1 > \beta_i > \beta_{i+1} > 0$, $0 < \alpha_i < \alpha_{i+1} < 1$ arises from the energy-momentum conservation, and within the DLA one can change it by the strong ordering eq.(2.13); this is the largest region which may give the DL-contribution.

Finally, the double logarithmic contribution of the diagram Fig.3 to the g_1 structure function is:

$$M_{3a} = - \left(\sum_q^{n_F} e_q^2 \right) 2C_F \left(\frac{\alpha_s}{2\pi} \right)^2 \int_x^1 \frac{d\beta_1}{\beta_1} \int \frac{d^2 k_{t1}^2}{k_{t1}^2} \frac{dk_{t2}^2}{k_{t2}^2}. \tag{2.20}$$

From this expression we extract the results for the transitions ΔP_{gq} and ΔP_{qg}:

$$\Delta P_{gq} = 2C_F, \tag{2.21}$$
$$\Delta P_{qg} = -2T_f. \tag{2.22}$$

It is interesting to note that the element corresponding to the gluon to quark transition (i.e. ΔP_{qg} splitting kernel) $-2T_f$ is negative. From the physical point of view it means that the slow (low x) produced quark has the helicity opposite to the one of the parent gluon; the initial gluon helicity goes to the fast antiquark with larger x.

At this point it may also be worthwhile to stress the change in the energy dependence of g_1 compared to the unpolarized case, where the longitudinal polarization of both t-channel gluons leads to the behavior $f_1(x) \propto 1/x$, i.e. to a singularity at angular momentum $j = 1$. In the present case we cannot have two longitudinally polarized t-channel gluons and therefore loose one power in $1/x$:

$$g_1(x) \sim x^0 \cdot F(ln(1/x)) \quad at \quad x \to 0. \tag{2.23}$$

Consequently, the rightmost singularity of the function g_1 in the complex angular momentum j-plane lies at $j = 0$. The t-channel quark exchange gives the same power of $1/x$ at small x, and therefore quark and gluon structure functions mix at small x. This is in contrast to the unpolarized case, where at small x the gluons dominate by one power in $1/x$.

To complete our discussion of the rungs, we have to adress the diagrams with gluon rungs in a gluon ladder. Such a contribution appears first in the 3^d loop, and it is illustrated Fig.4. To simplify the kernel we will write the triple-gluon vertex as a sum of three pieces (Fig.5a):

$$\Gamma_{\mu\nu\rho} = g_{\mu\nu}(k_1 + k_2)_\rho + g_{\mu\rho}(k_2 - 2k_1)_\nu + g_{\nu\rho}(k_1 - 2k_2)_\mu, \tag{2.24}$$

and note the following:
1) due to the antisymmentry in the indices $\mu'\nu'$ the graphs 5b,c do not contribute to g_1 (Fig.4);
2) due to gauge invariance we have $M_{\mu'\nu'}k_{1\mu'} = M_{\mu'\nu'}k_{1\nu'} = 0$ and $N_{\mu''\nu''}k_{2\mu''} = N_{\mu''\nu''}k_{2\nu''} = 0$;
3) graph Fig.5d does not give the leading logarithm, as the product $(k_1 + k_2)^2 = 2(k_1^2 + k_2^2)$ (note that the s-channel gluon $k_1 - k_2$ is on shell and $(k_1 - k_2)^2 = 0$; the term $\sim k_1^2$ (or k_2^2) cancels one of the gluon propagators and kills the logarithm $\frac{dk_t^2}{k_t^2}$ in the integral over k_{1t} (or k_{2t})). Thus the product of two triple gluon vertices in Fig.4 takes the form:

$$H_{\mu'\nu',\mu''\nu''} = 4 \left(\delta_{\mu'\mu''} k_{2\nu'} k_{1\nu''} + \delta_{\nu'\nu''} k_{2\mu'} k_{1\mu''} - \delta_{\mu'\nu''} k_{2\nu'} k_{1\mu''} - \delta_{\nu'\mu''} k_{1\nu''} k_{2\mu'}, \right) \tag{2.25}$$

which corresponds to the diagrams Fig.5c.

Together with the colour coefficient N_c it means that the insertion of an extra s-channel gluon into the gluon loop of Fig.3 leads to the double log integration

$$4N_c \frac{\alpha_s}{2\pi} \int \frac{d\beta_2}{\beta_2} \int \frac{dk_t^2}{k_t^2}. \tag{2.26}$$

Indeed, in order to keep the largest power of $1/x$ and to save the logarithm in the integrals over k_t we have to choose in (2.25) the transverse components of k_1 and k_2 and the longitudinal indices in $\delta_{\mu'\mu''}$, $\delta_{\nu'\nu''}$, $\delta_{\mu'\nu''}$ or $\delta_{\nu'\mu''}$. Such a configuration conserves the main structure of the gluon loop fig. 3, inserting instead of the spin part of the transverse gluon propagator $-e_{\nu'y}e_{\nu''y}$ (in Fig. 3) the expression $(e_{\nu''}k_{1t})(e_{\nu'}k_{2t}) = -|k_{1t} \parallel k_{2t}| \sin^2 \varphi$ (here φ is the angle between the transverse momenta k_1 and k_2 and we take into account the fact that $e_{\nu'} \perp k_{1t}$ and $e_{\nu''} \perp k_{2t}$). An additonal power of $|k_{1t}|$ and $|k_{2t}|$ comes from the traces of the lower and upper quark loops (like in the case of eq.(2.15)) and (2.16)). So after the integration over the azimuthal angle ($\langle \sin^2 \varphi \rangle = 1/2$) the vertex eq.(2.25) gives us the result (2.26) From this we extract the gluon rung ΔP_{gg}:

$$\Delta_{gg} = 4N_c = 4C_A \tag{2.27}$$

Finally, let us collect our results for the four different rungs. We define a matrix M_0 as illustrated in Fig.6, which contains the splitting functions ΔP_{ij}:

$$M_0 = \begin{pmatrix} 4C_A & -2T_f \\ 2C_F & C_F \end{pmatrix} \tag{2.28}$$

(here $C_A = N$, $C_F = \frac{N^2-1}{2N}$, and $T_f = \frac{n_f}{2}$ are the usual $SU(N)$ color factors; note that we have chosen to put the gluons into the first column and row). This matrix will be used in the following section where we shall derive the infrared evolution equations. For later purposes it will be convenient to consider also the color octet t-channel. In this case the color matrix analogous to (2.28) reads:

$$M_8 = \begin{pmatrix} 2C_A & -T_f \\ C_A & -1/2N \end{pmatrix}. \tag{2.29}$$

From our previous discussion we have also obtained the general pattern of the region of phase space which gives the double logarithmic contributions.The limits of integrations follow from the ordering condition given in eqs.(2.18),(2.19). In terms of β_i and k_{ti} it means that [15, 6]

$$k_{t,i+1}^2 \gg k_{t,i}^2 \frac{\beta_{i+1}}{\beta_i} \qquad (here \quad k_{ti}^2 > 0). \tag{2.30}$$

7

Indeed, let us first take $\beta_{i+1} \ll \beta_i$ and $k_{t,i+1} > k_{t,i}$. In this case $\alpha_{i+1} \approx \frac{k_{t,i+1}^2}{s\beta_i} \gg \alpha_i \approx \frac{k_{t,i}^2}{s\beta_{i-1}}$ (we have used the fact that s-channel partons with the momenta $k_i - k_{i+1}$ are on mass shell; $(k_i - k_{i+1})^2 \approx -k_{t,i+1}^2 - \alpha_{i+1}\beta_i s = 0$). On the other hand, if $k_{t,i+1} < k_{t,i}$ one has $\alpha_{i+1} \approx \frac{k_{ti}^2}{s\beta_i}$. In order to save the leading logarithm, we have to satisfy the condition: $k_{i+1}^2 \approx -k_{t,i+1}^2$, i. e. $\alpha_{i+1}\beta_{i+1}s \ll k_{t,i+1}^2$. In other words, our condition looks as

$$\tilde{\alpha}_{i+1} = \frac{k_{t,i+1}^2}{\beta_{i+1}s} \gg \frac{k_{ti}^2}{\beta_i s} \equiv \tilde{\alpha}_i \tag{2.31}$$

and as in [6] we can simply use the ordering eq.(2.19) with the $\tilde{\alpha}_i$ (eq.(2.31)) instead of the α_i.

In the final part of this section we have to consider nonladder diagrams as illustrated in Fig.7. We will call a non-ladder gluon "soft" if its transverse momentum is smaller than the momenta of all the partons comprised by the non-ladder gluon. According to Gribov's k_T-factorization theorem [7] [5] the whole amplitude of the 'soft' gluon emission can be written as the bremsstrahlung from one of the "external" lines of the block comprized by this gluon. Therefore the double logarithmic contribution coming from such a 'soft' gluons can be summed up with the help of the infrared evolution equation[8], in the same way as it was done for the non-singlet structure function g_1 in[4]. When summing over all possibilities of attaching the soft gluon to the external legs, we get a total color factor which depends on both the total t-channel color quantum number and the type of incoming partons. We will need the color singlet channel. For incoming gluons and fermions the color factors are C_A and C_F, resp. In matrix notation we define

$$G_0 = \begin{pmatrix} C_A & 0 \\ 0 & C_F \end{pmatrix}. \tag{2.32}$$

Finally we note that non-ladder gluons with k_t' larger than the transverse momenta in the part of the ladder, which is comprised by them (they will be called 'hard') do not give double logarithms. For a nonladder gluon that runs across the ladder from one side to the other (e.g. from the lower left to the upper right leg), the large momentum has to flow through some internal small k_{ti} ladder propagators, and the large momentum k_t' changes the normal $1/k_{ti}^2$ factor to $1/k_t'^2$, in this way killing the leading logarithm dk_{ti}^2/k_{ti}^2 (see Fig.7). These hard nonladder gluons therefore do not contribute to the double logarithmic approximation. Next we consider vertex correction (Fig. 7b). Then we can say that in the ultraviolet (large k_t') region there are no any double logs in the Feynmann gauge for the vertex function. So, one can anticipate that there are no DL-correction coming from large-k_t-region in the Feynmann gauge for the vertex function. However, we have to be more carefull here. For the unpolarized case there exists an example (BFKL) where a special cutting of the vertex-type diagram does give rise to a double log contribution. Indeed, let us consider the non-ladder on-shell gluon k' added to the amplitude: the loop integration yields $\frac{d^2k_t'd\beta'}{16\pi^3\beta'}$, two propagators —

[5]For QCD the Gribov's theorem was considered in more detail in [8, 7, 9] and [10]

$1/q^2 \approx \frac{1}{\alpha_q \beta' s}$, $1/k_2^2 \sim 1/k_{2t}^2$ and the spin part of the propagators, which for the nonsense, longitudinally polarization $(g_{\nu\nu'}^n \approx Q_\nu' p_{\nu'}/(Q'p))$ in the DL kinematical region $\beta_2 \ll \beta' \simeq \beta_1$ $(\alpha_q \gg \alpha')$ gives the factor $\simeq -(qp)(2k_1Q')/(pQ) \simeq \alpha_q \beta' s$. This factor cancels the propagator $1/q^2$, while the next propagator $1/k_{2t}^2 \sim \frac{1}{k_t'^2}$ provides the logarithmic integration $dk_t'^2/k_t'^2$ in the region $k_t' > k_{1t}$. As it is known [14], the sum of such contributions is equal to the ladder contribution (Fig. 4) but has an opposite sign. So it cancels the double logs coming from $k_t' > k_{ti}$ and restores the conventional DGLAP ordering $k_{t,i+1} > k_{t,i}$ for the gluon loops. Fortunately, this does not happen for the spin dependent structure function g_1. In this case the vertex of the "nonsense" gluon k' emission changes the sign, if unstead of the longitudinal polarizations of t-channel gluons k_1 and k_2 (in the left side of Figs.7c,d we consider the transverse polarization $e_1^t \perp k_{1t}$.[6]. Thus the amplitudes of the Fig.7 type, where the gluon k' is emitted one time by the transverse gluon and another time by the longitudinal one, cancel each other and we come back to the ladder configuration with the ordering eqs.(2.30), (2.31).

3 Infrared Evolution Equations

In this section we construct the infrared evolution equations which are necessary for the calculation of T_3 and g_1. We shall follow [4], and we begin with the amplitude T_3 which, following the discussion of the previous section, consists of the two components:

$$T_3 = \begin{pmatrix} T_3(\gamma^* g) \\ T_3(\gamma^* q) \end{pmatrix} \tag{3.1}$$

(from now on it will be understood that we consider the singlet part only, and we suppress the subscript "S".) The structure function then follows from the relation (2.3), and we have to take into account both DL-contributions and $i\pi$ -terms. We write T_3 as a Mellin transform:

$$T_3 = \int_{-i\infty}^{i\infty} \frac{d\omega}{2\pi i} (\frac{s}{\mu^2})^\omega \xi_{(\omega)} R(\omega, y), \tag{3.2}$$

where $R(\omega, y)$ is a two-component vector, defined on analogy to (3.1). The signature factor $\xi(\omega) =$ is:

$$= \frac{e^{-i\pi\omega} - 1}{2} \approx \frac{-i\pi\omega}{2}, \tag{3.3}$$

---

[6]To save logarithm in $d\beta'/\beta'$ integration the gluon k' should be the longitudinal, nonsense one; on the other hand the polarization vectors of the t-channel gluons k_1 (or k_2) and k_1 should be — one transverse and one longitudinal (for the small-x limit of g_1) as it was discussed just before eq. (11). If the vector $e_1 \parallel p$ than the leading contribution comes from the graphs Fig.7e,f and $\Gamma_{\mu\nu\rho} \cdot p_\mu Q_\nu' Q_\rho'/(pQ') \simeq -\frac{k_1Q'}{pQ'} = -\alpha_1$, while for the transverse vector $e_1 = e_{1t} = e_{2t}$ only the diagram Fig.7e do work and $\Gamma_{\mu\nu\rho} e_{1t\mu} e_{2t\nu} Q_\rho'/pQ' \approx +\alpha_1 + O(\alpha_2); \quad (\alpha_2 \ll \alpha_1)$.

and

$$y = \ln(\frac{Q^2}{\mu^2}). \tag{3.4}$$

Thus

$$-\mu^2 \frac{\partial R}{\partial \mu^2} = (\omega + \frac{\partial}{\partial y})R. \tag{3.5}$$

Eq.(3.5) represents the left-hand side of the IREE for T_3 which is illustrated in Fig.8. The right hand side is obtained from the observation that the dependence upon the cutoff μ resides in the intermediate state with lowest virtuality (Fig.8): the μ-derivative of the amplitudes are equal to R times quark or gluon scattering amplitudes with the external legs having transverse momenta close to μ. We are thus lead to the definition of a quark-quark scattering amplitude for which we use an integral representation of the form (3.2). The partial wave will be denoted by F_{qq}. More general, we introduce the four amplitudes F_{qq}, F_{qg}, F_{gq}, and F_{gg}, and in analogy with (2.28) we combine them into the two by two matrix F_0

$$F_0 = \begin{pmatrix} F_{gg} & F_{qg} \\ F_{gq} & F_{qq} \end{pmatrix} \tag{3.6}$$

(it is the analogue to $f_0^{(-)}$ in [4]). In terms of this F_0, the vector evolution equation for R becomes (Fig.8):

$$(\omega + \frac{\partial}{\partial y})R = \frac{1}{8\pi^2}F_0 R. \tag{3.7}$$

In analogy with [4, 8] the evolution equation of F_0 has the form (Fig.9a):

$$F_0(\omega) = \frac{g^2}{\omega}M_0 - \frac{g^2}{2\pi^2\omega^2}G_0 F_8(\omega) + \frac{1}{8\pi^2\omega}F_0(\omega)^2. \tag{3.8}$$

Here we have used the the matrices M_0 and G_0 defined in the previous section. The second term on the rhs of (3.8) corres ponds to the gluon bremsstrahlung diagrams: in analogy to the matrix F_0 which carries color zero we define the matrix F_8 of color octet amplitudes (it is the analogue to $f_8^{(+)}$ in [4]). These amplitudes satisfy the evolution equation similar to (3.8):

$$F_8 = \frac{g^2}{\omega}M_8 + \frac{g^2 C_A}{8\pi^2\omega}\frac{d}{d\omega}F_8(\omega) + \frac{1}{8\pi^2\omega}F_8(\omega)^2. \tag{3.9}$$

The matrix M_8 is taken from the previous section, and the color factor C_A in front of the second term on the rhs is the analogue of the matrix G_0 in (3.8). The difference between C_A in (3.9) and G_0 in (3.8) is due to the fact that for the positive signature amplitude F_8 the sum of the two bremsstrahlungs diagrams (illustrated in Fig.9b) is independent of the type of the incoming partons, and the matrix of color factors G_8 becomes C_A times the unit matrix.

4 Solution of the evolution equation

The solution for g_1 is obtained by solving eq.(3.9) for F_8, then eq.(3.8) for F_0 and eq.(3.7) for R (the latter makes use of the Born approximation R_B as initial condition for R), and finally inserting R into (3.2). The final answer for T_3 is the two component vector:

$$T_3 = \int \frac{d\omega}{2\pi i} \left(\frac{1}{x}\right)^\omega \xi(\omega) \left(\frac{Q^2}{\mu^2}\right)^{F_0/8\pi^2} \frac{1}{\omega - F_0/8\pi^2} R_B \tag{4.1}$$

Let us go through these steps in somewhat more detail.

We begin with the equation for F_8. We first diagonalize the Born term, i.e. the matrix M_8. The eigenvalues are:

$$\lambda_8^{(\pm)} = \frac{2C_A - 1/2N}{2} \pm \frac{1}{2}\sqrt{(2C_A - 1/2N)^2 - 4C_A T_f}. \tag{4.2}$$

Let $e^{(+)}$ and $e^{(-)}$ denote the two eigenvectors of M_8 and $E_8 = (e^{(+)}, e^{(-)})$ the matrix composed of them. Then

$$M_8 = E_8 \hat{M}_8 E_8^{-1}, \tag{4.3}$$

where $\hat{M}_8 = diag(\lambda_8^+, \lambda_8^-)$. Consequently, eq.(3.9) becomes diagonal if we transform to $\hat{F}_8$:

$$F_8 = E_8 \hat{F}_8 E_8^{-1}. \tag{4.4}$$

The solutions for the two components of $\hat{F}_8$ are:

$$\hat{F}_8^{\pm} = Ng^2 \frac{\partial}{\partial \omega}\left(\ln e^{z^2/4} D_{p_\pm}(z)\right), \tag{4.5}$$

where D_p denotes the parabolic cylinder function with

$$p_\pm = \frac{\lambda_8^{(\pm)}}{N} \tag{4.6}$$

and

$$z = \frac{\omega}{\omega_0}, \quad \omega_0 = \sqrt{Ng^2/8\pi^2}. \tag{4.7}$$

With this solution for F_8 we return to the evolution equation (3.8) for F_0 which is solved by the (matrix-valued) expression:

$$\frac{1}{4\pi^2\omega} F_0 = 1 - \sqrt{1 - \frac{g^2}{2(\pi\omega)^2} M_0 + \frac{g^2}{4\pi(\pi\omega)^3} G_0 F_8} \tag{4.8}$$

11

This has to be substituted into the final formula (3.2) for T_3. The leading behavior at small x comes from the right-most singularity in the ω plane. Similar to the nonsinglet case, this singularity is due to the vanishing of the square root in (4.8), i.e. we need to determine the zeroes of the eigenvalues of the matrix under the square root. Similar to the discussion after (4.2), the diagonalization of this matrix is done by the matrix E_0 consisting of the two eigenvectors $e_0^{(+)}$ and $e_0^{(-)}$ of the matrix under the square root.

Let us first return to the eigenvalues of M_8 determining the asymptotic behavior of F_8. For four active flavors the eigenvalues are:

$$\lambda_8^\pm = 2.92 \pm 1.88 = \begin{pmatrix} 4.8 \\ 1.04 \end{pmatrix}. \tag{4.9}$$

Neglecting fermions one obtains $\lambda = 6$, whereas the pure fermionic case corresponds to $\lambda = -1/6$. Obviously, the larger of the two eigenvalues is not too far from the gluonic case.

The accurate values have to be found from a numerical computation of the parabolic cylinder function. Before we quote the results of such a calculation it may be instructive to discuss a few approximations. Turning to the square root expression in (4.8), we are searching values of ω (or z) for which one of the two eigenvalues of the matrix under the square root in (4.8) becomes zero. To obtain a first estimate, we simply neglect the term containing F_8 (the exact calculation will show that this approximation is not too bad): then we can diagonalize F_0 by simply diagonalizing M_0. The eigenvalues are

$$\lambda_0^\pm = \frac{1}{2}(4C_A + C_F) \pm \frac{1}{2}\sqrt{(4C_A + C_F)^2 - 16C_A C_F - 16C_F T_f} \tag{4.10}$$

with the corresponding eigenvectors:

$$e^{(+)} = \begin{pmatrix} 1 \\ x^{(+)} \end{pmatrix}, \quad x^{(+)} = \frac{\lambda_0^+ - M_{0\;11}}{M_{0\;12}} = \frac{\lambda_0^+ - 4C_A}{-2T_f} \tag{4.11}$$

$$e^{(-)} = \begin{pmatrix} x^{(-)} \\ 1 \end{pmatrix}, \quad x^{(-)} = \frac{\lambda_0^- - M_{0\;22}}{M_{0\;21}} = \frac{\lambda_0^- - C_F}{2C_F}. \tag{4.12}$$

For the diagonalization we need the matrix $E_0 = (e^{(+)}, e^{(-)})$ and its inverse

$$E_0^{-1} = \frac{1}{1 - x^+ x^-} \begin{pmatrix} 1 & -x^- \\ -x^+ & 1 \end{pmatrix}. \tag{4.13}$$

The two values of z are (for four active flavors):

$$z_s = \begin{pmatrix} 3.81 \\ 1.81 \end{pmatrix} \tag{4.14}$$

(the pure gluonic and fermionic cases give $z = 4$ and $z = 4/3$ resp.). With the eigenvalues

$$\lambda_0^\pm = \begin{pmatrix} 10.88 \\ 2.46 \end{pmatrix} \tag{4.15}$$

12

the matrix E_0 is found to be:

$$E_0 = \begin{pmatrix} 1 & 0.42 \\ 0.28 & 1 \end{pmatrix}. \tag{4.16}$$

For the partial wave $R(\omega, y)$ in (3.2) we obtain:

$$R(\omega, y) = E_0 \frac{1}{\omega - \hat{F}_0/8\pi^2} \left(\frac{Q^2}{\mu^2}\right)^{\hat{F}_0/8\pi^2} E_0^{-1} \begin{pmatrix} 0 \\ 2e_q^2 \end{pmatrix}. \tag{4.17}$$

Retaining in $\hat{F}_0$ only the leading upper component, we find for the behavior of R near the square root branch point at $\omega = \omega_s$:

$$R(\omega_s, y) \sim \frac{1}{1 - 0.12} \begin{pmatrix} 1 & -0.42 \\ 0.28 & -0.12 \end{pmatrix} \frac{2}{\omega_s} \left(\frac{Q^2}{\mu^2}\right)^{\omega_s/2} \begin{pmatrix} 0 \\ 2e_q^2 \end{pmatrix}. \tag{4.18}$$

The fact that the matrix elements in the rightmost column are both negative has the important consequence that the leading contribution at small x changes the sign relative to the input distribution. Finally,

$$g_1^S = \frac{\omega_s^{3/2}}{8\sqrt{2\pi}} \frac{\frac{2}{\omega_s} + \ln Q^2/\mu^2}{(\ln(1/x))^{3/2}} (\Delta g, \Delta\Sigma) R(\omega_s, Q^2) (\frac{1}{x})^{\omega_s} \left(1 + O(\frac{\ln^2 Q^2/\mu^2}{\ln 1/x})\right) \tag{4.19}$$

where the vector R is from (4.18), and the (transposed) vector $(\Delta g, \Delta\Sigma)$ represents the initial conditions of the gluon and quark polarized distributions. It should be kept in mind that here we have retained only the leading singularity ω_s of (4.14). With ω_0 from (4.7) and $\alpha_s = 0.18$ we find $\omega_s = z_s\sqrt{\alpha_s N_c/2\pi} = 1.12$.

Finally, taking into account also F_8 we quote the result of a numerical calculation. For the larger of the two z-values we find ($n_f = 4$):

$$z_s = 3.45 \tag{4.20}$$

(the pure gluonic case would have given $z = 3.66$). With ω_0 from (4.7) and $\alpha_s = 0.18$ we find

$$\omega_s = z_s\sqrt{\alpha_s N_c/2\pi} = 1.01, \tag{4.21}$$

and with $x^+ = 0.29$, $x^- = 0.43$

$$R(\omega_s, y) \sim \begin{pmatrix} 1.14 & -0.50 \\ 0.33 & -0.14 \end{pmatrix} \frac{2}{\omega_s} \left(\frac{Q^2}{\mu^2}\right)^{\omega_s/2} \begin{pmatrix} 0 \\ 2e_q^2 \end{pmatrix}, \tag{4.22}$$

i.e. the negative sign persists. The result for g_1 becomes:

$$g_1(x, Q^2) = \frac{\omega_s^{3/2}}{8\sqrt{2\pi}} \frac{\frac{2}{\omega_s} + \ln Q^2/\mu^2}{(\ln(1/x))^{3/2}} (\Delta g, \Delta\Sigma) R(\omega_s, y) (\frac{1}{x})^{\omega_s} \left(1 + O(\frac{\ln^2 Q^2/\mu^2}{\ln 1/x})\right) \tag{4.23}$$

13

with R from (4.22).

Let us finally compare our result with the fixed order calculations. The region where we expect our result to coincide with the fixed order calculation is $\sqrt{\alpha_s} \ll \omega \ll 1$. We therefore expand our anomalous dimension matrix in powers of g^2/ω^2. To leading order we obtain:

$$\gamma_S^{(0)} = 2\frac{\alpha_s}{4\pi}\frac{1}{\omega}\begin{pmatrix} 4C_A & -2T_f \\ 2C_F & C_F \end{pmatrix}. \tag{4.24}$$

It agrees (as we have already mentioned before) with the singular part of [3, 11]. The next-to-leading-order matrix has the form:

$$\gamma_S^{(1)} = (\frac{\alpha_s}{4\pi})^2\frac{1}{\omega^3}\begin{pmatrix} 32C_A^2 - 16C_F T_f & -16C_A T_f - 8C_F T_f \\ 16C_A C_F + 8C_F^2 & 4C_F^2 - 16C_F T_f + \frac{8C_F}{N} \end{pmatrix}. \tag{4.25}$$

After transformation to x_B, it agrees with the leading powers on $\ln x$ given in eq.(3.65)-(3.68) of [12].

5 Discussion

The main result of this paper is the power-like behavior of the flavor singlet part of g_1 at small x (eq.(4.23)). The (leading) power is by a factor 2.6 larger than in the nonsinglet case. This effect is mainly due to the t-channel gluons states, which have a much larger color charge (cf.eq.(2.28), (2.29)) than the quarks (comparing the pure gluon and the pure fermionic case and neglecting the nonladder gluons one finds $\omega^{singlet}/\omega^{nonsinglet} = \sqrt{4C_A/C_F} = 3$). As it can be seen from a comparison of (4.14) and (4.20), the influence of the bremsstrahlung gluon is of the order of 10%. Comparing the flavor singlet with the nonsinglet, one notices that the nonladder bremsstrahlungs gluons act in quite different ways: in the present case, due to the positive sign of the largest matrixelemnt of M_8 ($M_{8\ 11}$), the leading ω-plane singularity moves to the left, i.e. the exponent of $1/x$ decreases from $\omega_s = 1.12$ to $\omega_s = 1.01$. For the flavor nonsinglet, on the other hand, the nonladder gluons lead to an increase of the exponent.

As to the polarization of the t-channel ladder gluons, the following pattern has emerged. In the unpolarized case, both t-channel gluons are longitudinally polarized (i.e. they are in the nonsense helicity state), and the resulting behaviour is $g(x, Q^2) \sim (1/x)^{1+O(\alpha_s)}$. In the polarized case, this leading contribution of gluon polarizations cancels, and the next-to-leading configuration appears: one gluon is still longitudinally polarized, but the other one has transverse polarization. The small-x behaviour is now of the form $g_1(x.Q^2) \sim (1/x)^{O(\sqrt{\alpha_s})}$. If both gluons are transversely polarized, the small-x behaviour is further suppressed: $\sim (1/x)^{-1+O(\sqrt{\alpha_s})}$. This contribution has been studied in [13].

Compared to the small-x prediction of the standard GLAP evolution equation, the main reason for the strong enhancement of our calculation lies in the different regions of phase space. Whereas in the GLAP case we have strong ordering in transverse momenta of the

14

ladder partons, our double logarithmic approximation has a much larger region of integration. A good way of illustrating the difference is the diffusion in $\ln k_T^2$ which first has been observed for the BFKL [14] Pomeron. When going, within ladder graphs, from one rung "i" to the next rung "i+1", ordering in transverse momenta means $k_{Ti} < k_{Ti+1}$. In the BFKL approximation, the distribution in $\ln k_{Ti+1}$ is a random walk distribution, i.e. when climbing up the ladder up to rung "i+1", we either add or subtract, at each step, a fixed steplength Δ. In the present double logarithmic approximation, on the other hand, the steplength is not fixed but can vary between zero and $\ln 1/x$. From this qualitative argument it is clear that, in the *polarized* case, the difference between the GLAP small-x behaviour and the double logarithmic prediction should be larger than, in the *unpolarized* case, the difference between GLAP and the BFKL behaviour.

Finally, at least a few words should be said about the phenomenological applications of our calculation [15, 16, 17]. Of particular interest is, of course, the question at what values of x and Q^2 the GLAP extrapolation should be replaced by the result of this paper. Leaving a more detailed discussion for future publications, we only want to make a few general remarks. In this paper we have derived expressions for Greens functions - $G_{q,g}(x, x'; Q^2, \mu^2)$ - which describe the evolution from the initial point (x', μ^2) to the final point (x, Q^2). If the initial polarized quark and gluon distribution do not exhibit any particularly strong variation in x, we can start from the approximation:

$$g_1(x, Q^2) = \Delta\Sigma(\bar{x}, \mu^2)G_q(x, \bar{x}; Q^2, \mu^2) + \Delta g(\bar{x}, \mu^2)G_g(x, \bar{x}; Q^2, \mu^2) \qquad (5.1)$$

where $\bar{x}$ denotes the mean x-value of the initial distributions. As a general feature, our Greens functions rather strongly depends upon the momentum scale μ^2.

Our analytic expression (4.23) represents only the leading term of the full amplitude (4.1). We have checked numerically that, as a function of x, the full amplitude (4.1) quickly shows the power behaviour predicted by the leading approximation (due to the factor $\ln 1/x$ there is, however, some difference in the overall normalization). Furthermore, as (4.22) suggests, at small x the gluon will dominate over the quark component. A numerical calculation shows that this, again, happens rather rapidly: the ratio of gluon and quark Greens functions G_g/G_q approaches its asymptotic value 3.45 approximately at $x = 10^{-3}$.

An important aspect of our result (4.23) is the sign structure. Our formula predicts that, at small x, the sign of g_1 should be opposite to that of the initial distributions. The experimental data [1] indicate that at small x the proton function $g_1^p(x)$ is positive, and even the neutron function g_1^n for $x < 0.01$ shows the tendency to change the sign and become positive. So, at first sight, there seems to be a problem. A possible way of resolving this conflict could be the following. Whereas the value of $\Delta\Sigma$ is known (and positive), we do not know the initial value of Δg. In ref.[18] it was shown that in a resonable model of the nucleon (non-relativistc quark or bag-model) this value may be negative, of about $\Delta g \sim -0.4$. Taking into account that at small x the gluon Greens function will dominate over the quark component, the structure function g_1 may very well become positive - both for the proton

and the neutron - and thus be consistent with the behavior observed in the data.

All these arguments are clearly very qualitative, and a more detailed quantitative analysis is of great importance. For the nonsinglet case, a first attempt has been made in [15] to estimate numerically how large the deviations of our double log formula from the usual GLAP predictions might be. Clearly any such estimate will strongly depend upon the input distribution. In [15] it was concluded that the deviations may be very large (up to an order of magnitude) but the difference between the nonsinglet $g_1(x, Q^2)$ and $f_1(x, Q^2)$ will not exceed 15 % within the HERA kinematical range. A somewhat different analysis has been performed in [17]. The situation with the singlet contribution will be more involved: not only is the power generated by the double logs larger than in the nonsinglet case, also the sign structure of the leading term (as mentioned in the previous section) will make the result more dependent upon the input. Clearly a careful study in this direction is strongly needed. On the longer run, also an improvement in accuracy of our double logarithmic approximation should be persued.

Figure Captions:

Fig.1: Born approximation for M^S.

Fig.2: First corrections to M^S: gluon rungs in the fermion ladder.

Fig.3: Lowest order contribution with t-channel gluons.

Fig.4: The first gluon rung.

Fig.5: Calculation of the gluon rung in Fig.4.

Fig.6: Matrix notation in Eq.(2.17).

Fig.7: Nonladder graphs.

Fig.8: Illustration of the infrared evolution equation (3.7).

Fig.9: (a) Illustration of the evolution equation (3.9); (b) origin of the color factor in front of the second term in (3.9).

References

[1] J.Ashman at el, EMC Collab., *Phys.Lett.* **B 206** (1988) 364; *Nucl.Phys.* **328** (1989) 1.
D.Adams et al., SMC Collab., *Phys.Lett.* **B329** (1994) 399; Erratum **329** (1994) 332.
B.Adeva et al., SMC Collab., *Phys.Lett.* **B302** (1993) 533; CERN-PPE-95/97 and
Phys.Lett. B 357 (1995) 248;
D.L.Anthony et al., SLAC-142 Collab., *Phys.Rev.Lett.* **71** (1993) 959; F.Staley, Proceedings of the International Europhysics Conference on High Energy Physics, Marseille 1993, (ed.J.Carr and M.Parrottet), p.114.
K.Abe et al., SLAC-143 Collab., *Phys.Rev.Lett.* **74** (1995) 346; *ibidem* **75** (1995) 25.

[2] V.N.Gribov and L.N.Lipatov, *Sov.Journ.Nucl.Phys.* **15**, 438 and 675 (1972).
Yu.L.Dokshitser, *Sov.Phys.JETP* **46** (1977) 641.

[3] G.Altarelli and G.Parisi, *Nucl.Phys.B* **126**, 297(1977).

[4] J.Bartels, B.I.Ermolaev, M.G.Ryskin, DESY-05-124 and Z.Phys.C, in print.

[5] B.L.Ioffe, V.A.Khoze, L.N.Lipatov, "Hard Processes", Noth-Holland, Amsterdam, 1984.

[6] V,N.Gribov, V.G.Gorshkov, G.V.Frolov, L.N.Lipatov, *Sov.J.Nucl.Phys.* **6** (1967) 95.
V.G.Gorshkov, *Sov.Phys.Yspekhi* **16** (1973) 322.

[7] V.N.Gribov, *Sov.J.Nucl.Phys.* **5** (1967) 280; B.I.Ermolaev, V.S.Fadin, L.N.Lipatov, *Sov.J.Nucl.Phys.* **45** (1985) 508.

[8] R.Kirschner and L.N.Lipatov, *Nucl.Phys.* **B 213** (1983) 122.

[9] B.I.Ermolaev and L.N.Lipatov, *Int.J.Mod.Phys.* **A4** (1989) 3147.

[10] M.Chaichian, B.I.Ermolaev, *Nucl.Phys.* **B 451** (1995) 194.

[11] M.A.Ahmed, G.G.Ross, *Nucl.Phys.* **B 111** (1976) 441.

[12] R.Mertig, W.Van Neerven, preprint INLO-PUB-6/95 and hep-ph/9506451.

[13] M.Fippel and R.Kirschner, *J.Phys.* **G 17** (1991) 421.

[14] E.A.Kuraev and L.N.Lipatov,V.S.Fadin, *Sov.Phys.JETP* **44** (1976) 443, *Sov.Phys.JETP* **45** (1977) 199;
Y.Y.Balitskij and L.N.Lipatov, *Sov.J.Nucl.Phys* **28** (1978) 822;
L.N.Lipatov, *Sov.Phys.JETP* **63** (1986) 904.

[15] B.I.Ermolaev, S.I,Manayenkov, M.G.Ryskin, DESY-95-017.

[16] M.Glück, E.Reya, M.Stratmann, W.Vogelsang, preprint DO-TH 95/13.

[17] J.Blümlein and A.Vogt, DESY 954-175.
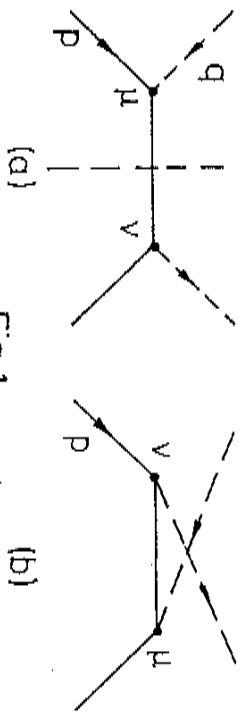
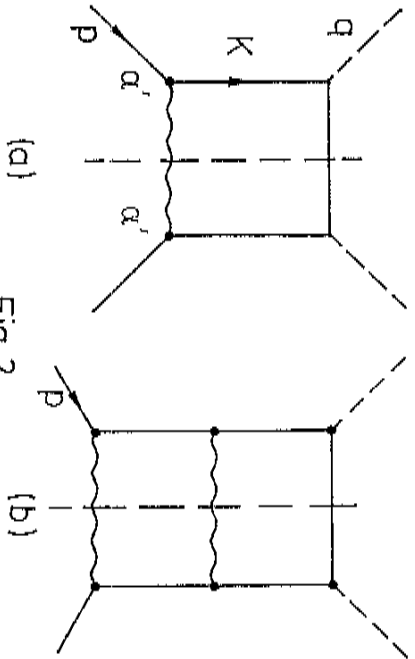[18] R.L.Jaffe, *Phys. Lett.* **B 365** (1996) 359.

Fig. 1

Fig. 2

Fig. 3
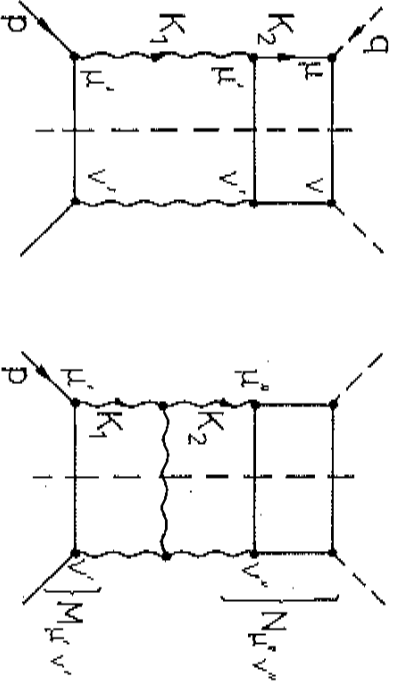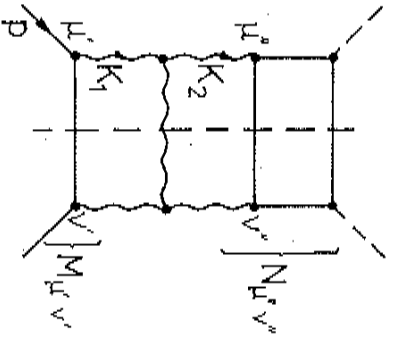
Fig. 4

Fig. 5

Fig. 7

(e)   +   (f)

(c) K_1 K_2 $\tilde{K}_1$ K'

(d) K_2 K'

(a) K' $K_{it}+K_i'$

(b) K'

$M_0 =$

Fig. 6

$$\mu^2 \frac{\partial}{\partial \mu^2} \left(\right) = \mu^2 \frac{\partial}{\partial \mu^2} \left(0 \right) + \mu^2 \frac{\partial}{\partial \mu^2} \left(\right)$$

Fig. 8

$$\mu^2 \frac{\partial}{\partial \mu^2} \left(0 \right) = \mu^2 \frac{\partial}{\partial \mu^2} + \mu^2 \frac{\partial}{\partial \mu^2} + \mu^2 \frac{\partial}{\partial \mu^2} \left(\infty \right) + \mu^2 \frac{\partial}{\partial \mu^2} \left(0 \quad 0 \right)$$

(a)

$$\left(\infty \right) + \left(\infty \right)$$

(b)

Fig. 9